Numerical study of the flow field around spheroidal particles

Mohamed Chekired & Varvara Roubtsova
Hydro-Québec, Varennes, Québec, Canada
Elham Kheradmand, Serge Prudhomme, & Marc Laforest
Département de mathématiques et de génie industriel – École Polytechnique de Montréal, Montréal, Québec, Canada

ABSTRACT
A research program was initiated to provide key microscopic information about the field surrounding ellipsoidal particles and gain a better insight into granular media under earthquake conditions. Numerical studies of steady streaming flows are presented for spheroidal particles oscillating in a viscous fluid. Several aspect ratios and angular positions of the spheroids were studied with respect to the Reynolds number. The results were compared with the published experimental data of Kotas et al. (2006). Additional simulations were performed to verify the predicted value of the drag force acting on ellipsoids in creeping, laminar, and separated flows. Results of the simulations were compared with a correlation formula based on a large volume of experimental data published by Hölzer and Sommerfeld (2008). A discussion on the use of ellipsoidal particles for computer simulations of soil behavior at the micro scale concludes the article.

RÉSUMÉ
Un programme de recherche a été établi pour fournir des informations clés à l'échelle microscopique du champ entourant les particules ellipsoïdales et obtenir ainsi un meilleur aperçu des milieux granulaires sous sollicitations sismiques. Des études numériques d'écoulements stationnaires sont présentées pour des particules sphéroïdales oscillant dans un fluide visqueux. Plusieurs rapports de diamètres et positions angulaires de particules sphéroïdes ont été étudiés par rapport au nombre de Reynolds. Les résultats ont été comparés aux données expérimentales publiées de Kotas et al. (2006). Des simulations supplémentaires ont été effectuées pour vérifier la valeur prédite de la force de traînée agissant sur les ellipsoïdes dans les écoulements rampants, laminaires et décollés. Les résultats des simulations ont été comparés avec une formule de corrélation basée sur un grand volume de données expérimentales publiées par Hölzer et Sommerfeld (2008). Une discussion sur l'utilisation de particules ellipsoïdales pour des simulations informatiques du comportement du sol à l'échelle micro conclut l'article.

1 INTRODUCTION

The motion of particles in viscous fluids plays an important role in soil science and river mechanics, involving, for instance, such phenomena as sediment transport, erosion, sedimentation, liquefaction and slopes stability. The presence of moving particles causes changes in the flow field characteristics through pressure and velocity. The liquid also influences the moving particles by the addition of a hydrodynamic force resulting from the pressure and viscosity fields acting on individual particles. Modeling of this process has mostly relied to date as per previous studies on spherical particles (Fries et al., 2011, Zhao et Shan 2013, Kloss et al., 2012). However, actual soil particles are usually non-spherical and their motion can be strongly affected by their shape.

Flow is governed by the incompressible Navier-Stokes equations and particle interactions obey Newton's laws. In this study, simulations were performed using SiGran, a virtual laboratory that was developed at the Research Institute of Hydro-Quebec (IREQ). SiGran is based on coupling of two methods: the Marker and Cell (MAC) method and the Discrete Element Method (DEM). The MAC method is a robust method that models unsteady flows ranging from creeping flows to high Reynolds number flows. DEM was designed to simulate interactions between particles. More details about SiGran can be found in Roubtsova et al. (2015), which focused on an energy balanced DEM method using SiGran. Simulations to analyze specific properties of channel flows at the pore scale are also described in Chekired and Roubtsova (2014).

Three-dimensional numerical simulations using MAC and DEM are computationally intensive, due to the need to process large numbers of interparticle contacts when dealing with dense soils and to solve the Poisson's equation for the fluid pressure within the complex geometry of pore channels at each time step, which requires access to substantial computing resources. In order to keep both simulation time and computational resource requirements to a minimum, the model was parallelized using GPUs (Graphics Processing Units). For portability, the OpenCL (Open Computing Language) framework was used, which offers an abstract view of the parallel architecture. This allows one to take advantage of both the CPU (Central Processing Units) and the GPU backend (Roubtsova et al., 2012).

2 FLOW MODELING

The basic equations governing the flow of an incompressible fluid are as follows. Conservation of momentum is satisfied by:

$$\rho\left(\frac{\partial \vec{v}}{\partial t} + (\vec{v}\cdot\nabla)\vec{v}\right) = -\nabla \mathrm{p} + \eta\nabla^2\vec{v} \qquad [1]$$

where ρ is the density of the liquid (kg/m^3), t is the time (s), $\vec{v}$ is the flow velocity (m/s), p is the pressure (Pa), and η is the dynamic viscosity (Pa·s). Continuity is given by:

$$\nabla \cdot \vec{v} = 0 \qquad [2]$$

The Marker and Cell (MAC) method is employed to approximate these equations. The method was developed by Harlow and Welch (1965) for the simulation of free surface flows. Based on a structured and staggered grid system (Figure 1), the MAC method is a finite difference solution technique for investigating the dynamics of an incompressible viscous fluid. The primary dependent variables are pressure and velocity. The pressure variable is evaluated at the center and the velocity on the faces of the cells, respectively.

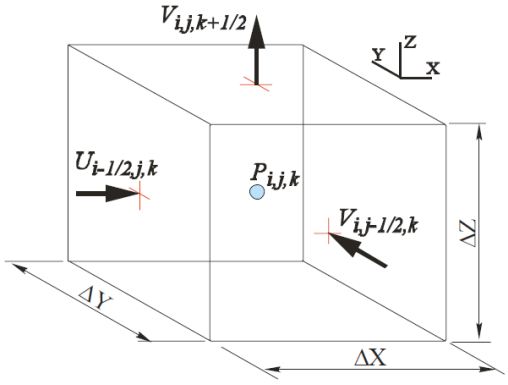

Figure 1. 3D MAC grid cell

Boundary conditions along solid walls are prescribed as non-slip and non-penetration conditions. The grids are constructed so that the grid points corresponding to the normal velocity components lie on the walls. To calculate the parallel velocity components, a special approximation near the walls for temporal velocity is employed (Belotserkovsky, 1994). This method prevents the addition of fictive layer cells in each particle which is necessary in MAC and SMAC schemes. Boundary conditions for the pressure is of the Neumann type. At the inflow boundaries, one prescribes the normal velocity component while the other components are set to zero. Finally, free boundary conditions are prescribed at the outflow boundaries.

The force due to the flow around a particle is estimated by integrating the pressure-viscous stress tensor over the particle surface:

$$\vec{F} = \oint_S (-pI + \tau) \cdot \vec{n} dS \qquad [3]$$

where $\vec{F}$ is the hydrodynamic force (N) that accounts for the drag, lift, and buoyancy forces, I is the identity matrix, $\vec{n}$ is the unit normal vector to the particle surface, S denotes a particle surface (m^2), and τ is the viscous stress tensor (Pa):

$$\tau = \eta(\nabla v + \nabla v^T) \qquad [4]$$

Note that the stress tensor depends only on the pressure and the strain tensor and is independent of the antisymmetric vorticity terms (Landau and Lifschitz, 1959).

3 OSCILLATING ELLIPSOIDAL PARTICLES

Liquefaction is the phenomenon by which the strength and stiffness of a saturated soil is reduced by earthquake shaking or other rapid loading.

During the cyclic loading process, the particles oscillate and generate a specific surrounding flow field. Adequate simulation of the flow around an oscillating particle constitutes the first step in the modeling of the liquefaction process at the micro scale, i.e. the scale at which the problem is described in terms of individual particles that interact with each other and with the fluid.

Experimental studies of steady streaming flows near oscillating ellipsoidal particles were carried out by Kotas et al. (2007). In these experiments, the particles had a maximum dimension of 2.54 cm and were immersed in a 25 x 50 x 30 cm glass tank containing a working fluid (10% water and 90% glycerin by weight). The kinematic viscosity and density of the fluid were 1.69x10^{-4} m^2/s and 1.23 g/cm^3, respectively. The particles were glued to 0.2 or 0.4 cm diameter stainless steel mounting rods passing through the center of the particles and rigidly mounted to the table of an electrodynamic shaker subjected to sinusoidal oscillations.

SiGran considers uniform grids, which is pertinent for the typical geotechnical problems for which the code was written. From previous numerical studies using SiGran, the pore-channels require at least five MAC-cells by width in order to adequately calculate the flow. On the other hand, each particle must be surrounded by at least 10 MAC-cells in order to obtain a good integration of the drag force. Usually the pore channels are evenly distributed in a soil sample, meaning that the same grid should be used to simulate all samples with the same precision. This is usually the case for applications involving seepage, permeability, or stress-strain tests. Another type of problem in soil science is that of large displacements of soil particles under flow forces. In this case, the evolution of particles cannot be predicted a priori and adaptation of the grid during the simulation may require more time than simply discretizing the full domain with a fairly fine grid. This is in particular the case when considering erosion, liquefaction, or sediment settling problems. There are exceptions to these typical problems. The shear stress test is one where the region of interest is a small layer along a shear surface. Another example is surface erosion where the zone of interest is a boundary layer between the soil and the fluid.

The problem of simulating an oscillating particle in a large box is not a typical problem for SiGran. The flow field around the particle consists of inner and outer regions rotating in opposite directions (see Figure 2).

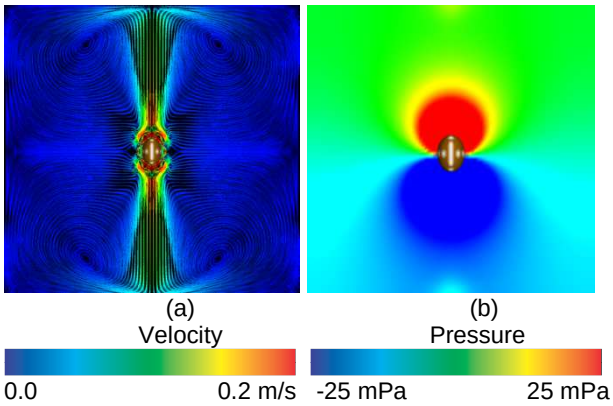

Figure 2. (a) numerically determined steady streaming flows and (b) pressure field around a vertically oscillating spheroidal particle.

The size of the inner region depends on the Reynolds number calculated from maximal velocity during oscillation as follows:

$$Re = 2\pi f AD/\mu \qquad [5]$$

where f is the oscillating frequency (Hz), A is the oscillating amplitude (m), D is the typical body length scale (m), and μ is the kinematic viscosity (m^2/s).

Comparison of the simulation results with published experimental data was carried out for the inner regions only. Plotting the streamlines near a particle was indeed challenging because of the staggered grid system.

The algorithm proposed by Mogilenskikh and Pavlov (2002) was used to draw the streamlines. The particularity of SiGran is that the algorithm is implemented in parallel: all lines that have the same vertical coordinate at start point are calculated simultaneously. The approximation of the velocity at point (x, y) is presented in Figure 3. As previously mentioned the particle boundary which coincides with the cell walls gives non smooth surface of particle and complicates the streamlines drawing.

Results for an ellipsoidal particle with major axis equal to 2.54 cm and the other two axes equal to 1.905 cm are shown in Figure 4. Here, the Reynolds number is set to 40 and the oscillation amplitude is 0.5 cm.

A second example deals with an obliquely oscillating ellipsoidal particle with a major axis equal to 2.54 cm and the other two axes equal to 1.27 cm. The Reynolds number is set to 10 and the oscillation amplitude is 0.5 cm. The authors (Kotas et al. 2007) noted that the oblique oscillation destroys the axisymmetric configuration of the flow. Rotation of the oscillating particle also induces a rotation of the inner region but at a lesser angle than that of the particle. Figure 5 compares the experimental streamlines with those obtained from the simulations.

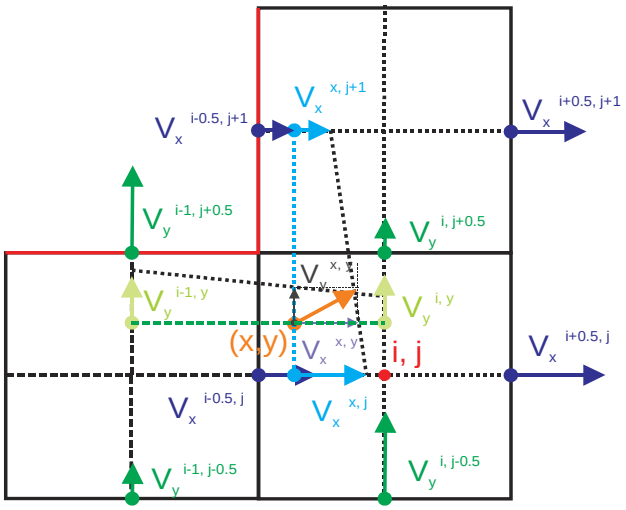

Figure 3. Schematic of the velocity approximation for streamline tracing in the 2D case.

- Centre of MAC grid (i, j)
- i,j — Horizontal and vertical numbers of MAC-grid
- Point of interest with coordinates (x, y)
- Particle boundary
- X component of velocity in point of MAC grid
- Y component of velocity in point of MAC grid
- X component of velocity for points with (x) coordinate at center of MAC grid
- Y component of velocity for points with (y) coordinate at center of MAC grid
- X component of velocity for point (x, y)
- X component of velocity for point (x, y)
- Velocity at point (x, y)

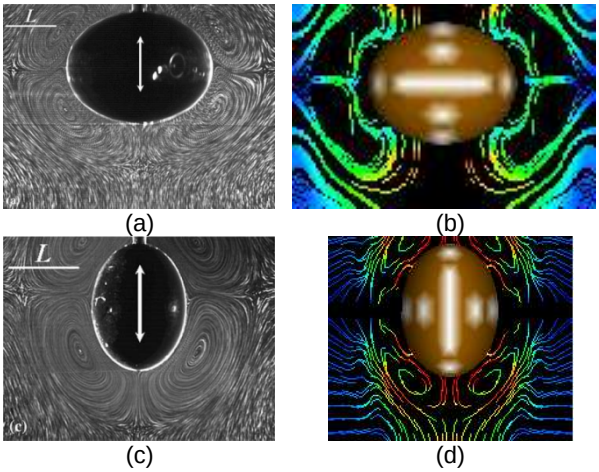

Figure 4. Streamlines around ellipsoidal particles that oscillate in the vertical direction. (a), (c): Experimental data obtained by Kotas et al. (2007) and reproduced with permission from Springer International Publishing; (b),(d): Numerical results obtained with SiGran.

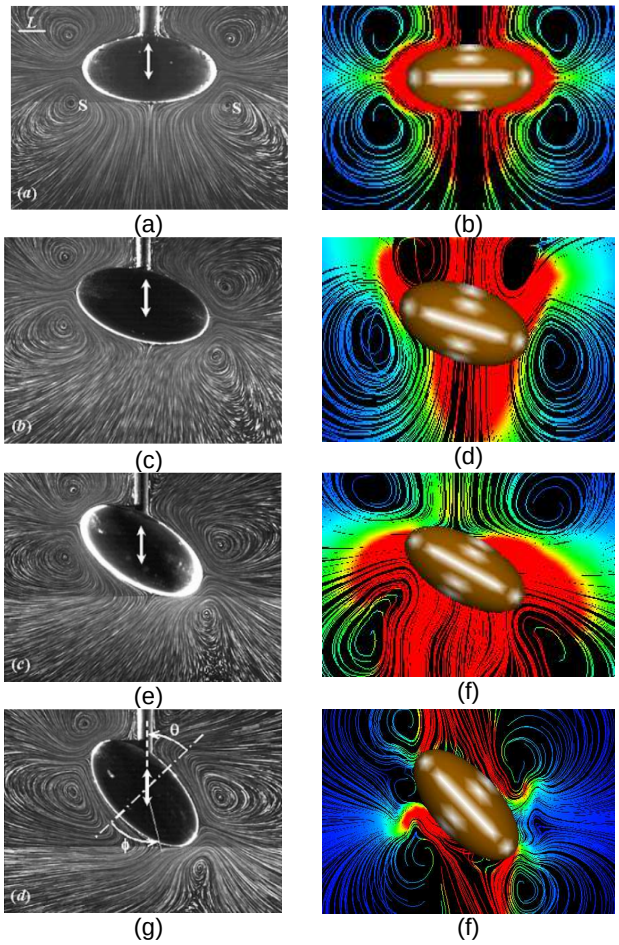

Figure 5. Streamlines around ellipsoidal particle oscillating in the vertical direction. (a), (c), (e), (g) show the experimental data obtained by Kotas et al. (2007) and reproduced with permission from Springer International Publishing. (b), (d), (f), (h) show the numerical data obtained with SiGran. The angular position was measured counterclockwise as shown in (g): (a), (b) $\theta = 0^o$; (c), (d) $\theta = 15^o$; (e), (f) $\theta = 30^o$; (g), (h) $\theta = 45^o$.

Differences between the simulated and experimental streamlines can be explained by the presence of the rod in the experiment, phase lag between the experiments and numerical simulations (i.e. the particles were not at the center of oscillation), and discretization errors due to the SiGran grid, as discussed above.

For the time being, the current simulations of oscillating ellipsoidal particles have put in evidence a new issue, namely, that of reducing the numerical viscosity of the numerical scheme. This is crucial due to the fact that the fluid in geotechnical processes usually consists of water. Water has a small viscosity, about 1 mPa.s at 20°C, which is comparable to the numerical viscosity. One way to improve the dissipative properties of the numerical scheme is to use a High Resolution Scheme (HRS) for the discretization of convective flows (Volkov, 2004).

4 DRAG COEFFICIENTS FOR ELLIPSOIDAL PARTICLES

The flow around a particle creates a hydrodynamic force that affects the motion of the particle. This force depends on the velocity (see Figure 2a) and pressure (see Figure 2b) flow fields, the liquid viscosity, the particle shape and size, and its orientation relative to the flow direction. As was noted above, SiGran calculates this force directly by integrating the viscous and pressure stress tensors around the particle (see Eq. [3]).

Usually, the hydrodynamic force includes three contributions according to their action on the particle: buoyancy, lift, and drag forces. Note that the lift and drag forces can induce a moment to the particle since their resulting forces do not necessarily pass through the center of mass of the particle. Buoyancy force results from the difference between the action of the gravity hydraulic pressure and the gravity force. Lift force is the component of the hydrodynamic flow force that is normal to the incoming flow direction and is created by a non-symmetric flow around the particle. Drag force is the component of the hydrodynamic flow force that is parallel to the incoming flow. The components that most influence the motion of the particles depend on their shape and their position with respect to the flow as well as the dynamic viscosity of the fluid and the flow velocity. At small Reynold numbers, the drag force is greater. The non-symmetrical shape of the particle relative to the oncoming flow can create a significant lift force while a perfect symmetry reduces this force to zero. Here only the drag force is analyzed.

The drag coefficient C_D is a dimensionless quantity derived from the drag force as:

$$C_D = \frac{|F_D|}{0.5\rho u^2 S} \qquad [6]$$

where F_D is the drag force (N) acting on the particle, u is the flow speed of the particle relative to the fluid (m/s), S is the reference area of the particle (m^2). The reference area is usually chosen as the largest cross-sectional area perpendicular to the flow. The relative speed is a questionable value because the velocity of the flow around the particle can greatly vary. The incoming or far-field speed is used for the flow value in Eq. [6]. The analytical solution for the drag force of a particle is only available for spheres and ellipsoids at low Reynolds numbers (Stokes flow with Re ≤ 1) (Stokes 1851, Lamb 1916).

A new simple correlation formula [7] for the standard drag coefficient (i.e. a single stationary particle of arbitrary shape in a uniform flow) was established by Hölzer and Sommerfeld (2008) using a large set of experimental data from the literature and a comprehensive numerical study:

$$C_D = \frac{8}{Re}\frac{1}{\sqrt{\Phi_{||}}} + \frac{16}{Re}\frac{1}{\sqrt{\Phi}} + \frac{3}{\sqrt{Re}}\frac{1}{\Phi^{\frac{3}{4}}} + 0.4210^{0.4(-\log\Phi)^{0.2}}\frac{1}{\Phi_{\perp}} \qquad [7]$$

where Φ is the sphericity, which represents the ratio between the surface area of the volume equivalent sphere

and that of the considered particle, $\Phi_{||}$ is the lengthwise sphericity, which is the ratio between the cross-sectional area of the volume equivalent sphere and the difference between half the surface area and the mean projected longitudinal cross-sectional area of the considered particle, $\Phi_{\perp}$ is the crosswise sphericity, which is the ratio between the cross-sectional area of the volume equivalent sphere and the projected cross-sectional area of the considered particle. This correlation formula considers the particle orientation over the entire range of Reynolds numbers and has known limits of applicability with respect to the sphericity. The mean relative deviation between formula [7] and 2061 experimental data from the literature for a variety of particle shapes is 14.1%. For more details about this formula, see Hölzer and Sommerfeld (2008).

The first term in formula [7] stands for the pressure or form drag associated with the lengthwise sphericity, the second term stands for the friction drag associated with the surface area. These two terms dominate the drag force in the Stokes region (see Figure 4). In the case of a sphere, the three sphericity parameters defined above are all equal to unity and the sum of these two contributions is then identical to the Stokes analytical solution for the drag coefficient. The last two terms are provided in terms of the correlation formula at high Reynolds numbers. The graphical representation of these terms and comparison between formula [7] and the SiGran numerical simulation for a spherical particle are shown in Figure 6.

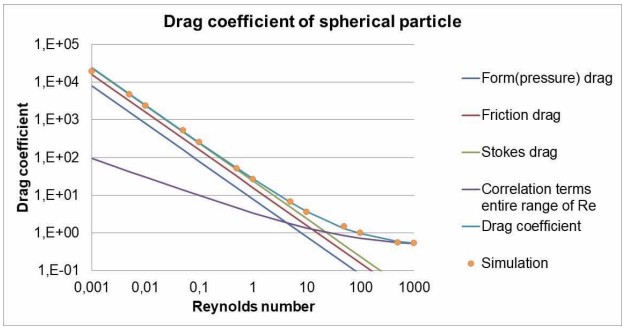

Figure 6. Comparison between the correlated and the numerically obtained drag coefficients of spheres.

Comparison of the drag coefficient obtained by formula [7] and by numerical simulation in the case of an ellipsoidal particle whose major axis is either parallel (ellipsoid 1) or perpendicular (ellipsoid 2) to the incoming flow is shown in Figure 7. The geometrical data for the spherical particle of Figure 6 and for the ellipsoids of Figure 7 are collected in Table 1.

The streamlines for a variety of particle shapes at different Reynolds numbers are shown in Figures 8-10 for laminar and separated flows.

Table 1. Geometrical characteristics of particles

Characteristics		Sphere	Ellipsoid 1	Ellipsoid2
semi-axis, (mm)	a	5	5	
	b	5	3	
	c	5	1	
Volume of ellipsoid, (mm^3)		523	62.8	
Rayon of equivalent sphere, (mm)		5	2.4	
Surface area of equivalent sphere, (mm^2)		314	76.4	
Sections area of equivalent sphere, (mm^2)		78.5	19.1	
Surface area of ellipsoid, (mm^2)		314	109	
Crosswise section area of particle, (mm^2)		78.5	47.1	94.2
Lengthwise section area of particle, (mm^2)		78.5	94.2	47.1
Sphericity		1	0.7	
Crosswise sphericity		1	0.41	0.42
Lengthwise sphericity		1	2.03	2.57

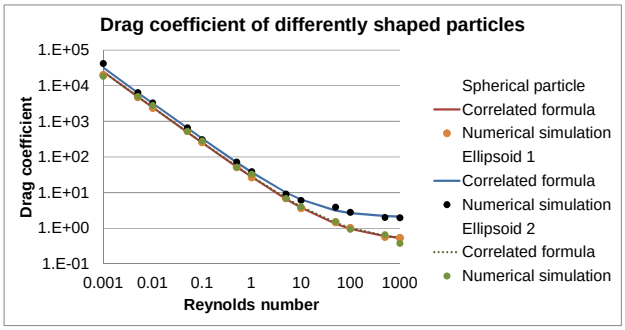

Figure 7. Comparison between the correlated and the numerically obtained drag coefficients of differently shaped particles.

5 CONCLUSIONS AND FUTURE WORK

SiGran was used earlier for investigating a series of different geotechnical problems. For example, the full work-energy balance during shear-stress tests was analyzed by Amirpour et al., (2017) using SiGran simulations. In this article the transformation of energy for each particle into shear-box was analyzed and the inter-particle mechanism that absorbs more energy at a shear plane was observed. The algorithm for the creation of virtual soil samples with desired density and a particle size-distribution was written by Roubtsova and Chekired (2014). In this work, a virtual sample was used to determine the soil permeability and a direct calculation of tortuosity. All these results were obtained in the case of spherical particles.

With current developments in mathematical and computational sciences, it is now possible to consider simulations with ellipsoidal particles, one step closer to solving actual problems. The main issue when dealing with ellipsoidal particles is to identify the contact point

using a reasonable number of iterations when solving the corresponding non-linear problems. This means that the time of calculation must remain acceptable for engineering problems of practical interest.

The present work has focused on the behavior of individual ellipsoidal particles within a fluid flow. Experimental and numerical results have shown reasonable agreement with respect to the streamline patterns and values of the drag force coefficient. Further studies are being planned in order to continue the analysis of the interaction of ellipsoidal particles in a viscous fluid. SiGran is capable to simulate the influence of one particle motion on the hydrodynamic force of another particle by a flow perturbation thanks to the direct integration of this force and a precise calculation of the flow around particles. We also mention that the rotation of ellipsoidal particles perturbs the surrounding flow more than in the case of spherical particles. Hence, the flow around the elliptical particles exhibits more complex patterns than around spherical particles.

This study has also puts in evidence some shortcoming of SiGran, in particular the presence of numerical viscosity. This aspect is very important for liquefaction simulations where the particles oscillate in a very small closed volume**.** Higher-order numerical schemes will be considered in order to solve this issue.

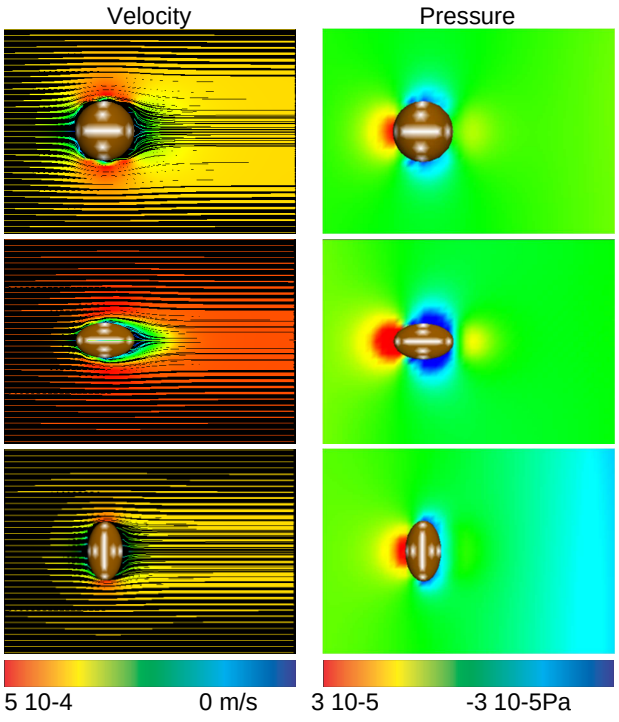

Figure 8. The streamlines and pressure fields around spherical and ellipsoidal particles in a Stokes flow (Re = 0.5).

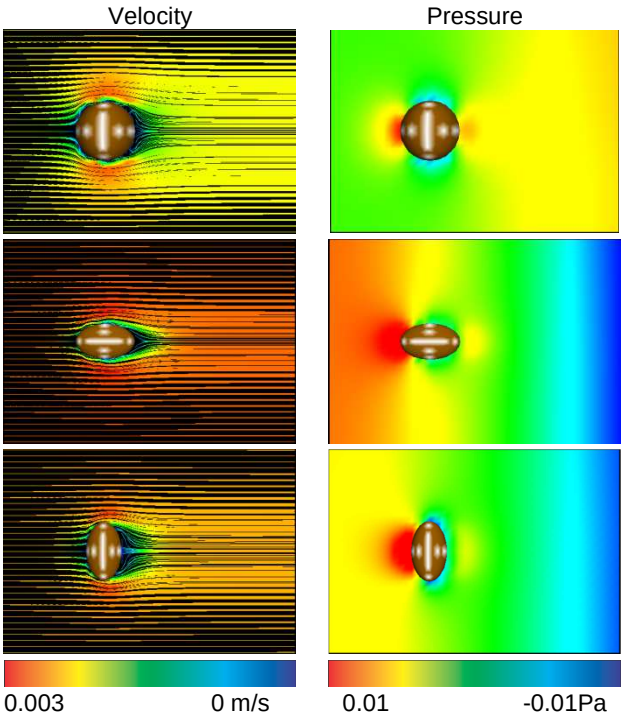

Figure 9. The streamlines and pressure fields around the spherical and ellipsoidal particles in a laminar flow (Re = 25).

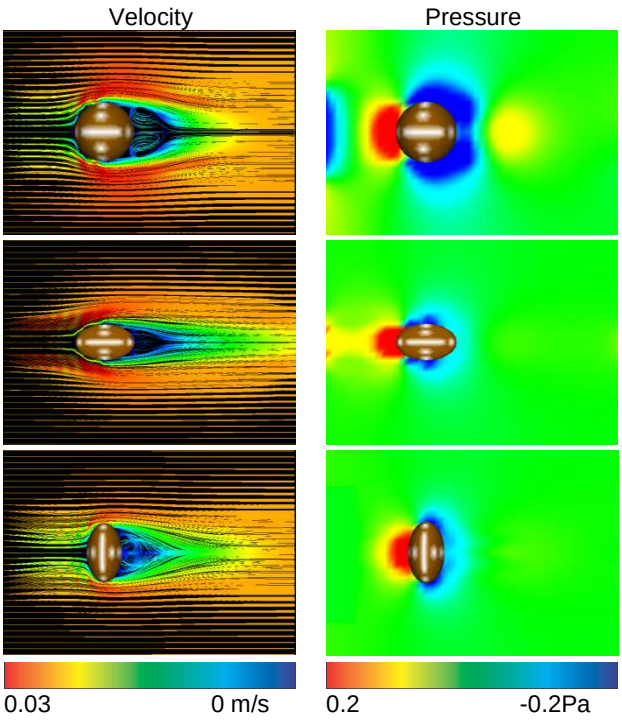

Figure 10. The streamlines and pressure fields around spherical and ellipsoidal particles in a separated flow behind the particles (Re = 250).

REFERENCES

Amirpour, S., Roubtsova, V., Chekired, M., Hussien, M. N., Karray, M., 2017. Micromechanics-based assessment of reliability and applicability of boundary measurements in symmetrical direct shear test, *Canadian Geotechnical Journal*

Belotserkovsky, O.M., 1994. Numerical modeling in the mechanics of continuous media, Moscow: Physico-mathematic literature (in Russian)

Chekired, M. and Roubtsova, V., 2014. Pore-scale study of permeability and tortuosity for flow through particulate media using virtual approach, *ICSE-7, 7th International Conferences on Scour and Erosion*, Perth, Australia, December 2-4.

Chekired, M., Roubtsova, V., Kheradmand, E., Prudhomme S., and Laforest, M.,(2017) DEM simulation with elliptical particles for micro-level geotechnics simulations, *70th Canadian Geotechnical Conference,* Ottawa, Canada, October 1-4

Fries, L., Antonyuk, S., Heinrich, S. and Palzer, S., 2011 DEM-CFD modeling of a fluidized bed spray granulator, Chemical Engineering Science vol. 66 pp. 2340-2355

Harlow, F.H. and Welch, J.E., 1965. Numerical calculation of time-dependent viscous incompressible flow of fluid with a free surface, *The Physics of Fluids,* vol. **8**, pp. 2182-2189.

Hölzer, A. and Sommerfeld, M., 2008. New simple correlation formula for the drag coefficient of non-spherical particles, *Powder Technology*, 184: 361-365.

Kloss, C., Goniva, C., Hager, A., Amberger, S. and Pirker S., 2012 Models, algorithms and validation for pensource DEM and CFD-DEM, *Progress in Computational Fluid Dynamics, Vol. 12, Nos. 2/3,* 140-152

Kotas, C.W., Yoda, M. and Rogers, P.H., 2007. Visualisation of steady streaming near oscillating spheroids, *Exp Fluids,* 42: 111-121.

Lamb, H., 1916. *Hydrodynamics*, Cambridge: Cambridge University Press.

Landau, L.D. and Lifschitz, E.M., 1959. *Course of Theoretical Physics,* Vol. 6 Fluid Mechanics, Oxford: Pergamon Press.

Mogilenskikh, D, V, and Pavlov, I.V., 2002, Color interpolation algorithms in visualizing results of numerical simulations. *Visualization and imaging in transport phenomena. Annals of the new tork academy of sciences. vol. 972,* p.43-52.

Roubtsova, V., Chekired, M., Karray, M. and Amirpour, S., 2015, Work-energy balance for discrete element method using shear stress tests, *Congress on Numerical Methods in Engineering (CMN 2015)*, Lisbon, Portugal, 29 June - 2 July.

Roubtsova, V., Morin, B., Chekired, M., 2012. Parallel algorithm for fractal scaling of soil particle-size distributions. *High Performance Computing Symposium* (HPCS2012), Vancouver, Canada, May 1-3.

Roubtsova, V., and Chekired M., 2014. 3D numerical simulations of particle-water interaction using virtual approach, *SimHydro 2014: Modelling of rapid transitory flows*, Sophia Antipolis, June 11-13.

Stokes, G.G., 1851. On the Effect of the Internal Friction of Fluids on the Motion of Pendulums. *Transactions of the Cambridge Philosophical Society*, Part II, 9, 8-106.

Volkov K. N., 2004, Discretization of convective fluxes in Navier-Stokes equations on the basis of high-resolution difference schemes, Vychisl. Metody Programm., Volume 5, Issue 1, 129–145 *(in Russian)*

Zhao, J. and Shan, T. 2013 Coupled CFD–DEM simulation of fluid–particle interaction in geomechanics, *Powder Technology,* vol. 239, pp. 248-258